LETTERS

# Mechanism of folding chamber closure in a group II chaperonin

Junjie Zhang[1,2], Matthew L. Baker[2], Gunnar F. Schröder[3]†, Nicholai R. Douglas[4], Stefanie Reissmann[4]†, Joanita Jakana[2], Matthew Dougherty[2], Caroline J. Fu[2], Michael Levitt[3], Steven J. Ludtke[1,2], Judith Frydman[4] & Wah Chiu[1,2]

**Group II chaperonins are essential mediators of cellular protein folding in eukaryotes and archaea. These oligomeric protein machines, ~1 megadalton, consist of two back-to-back rings encompassing a central cavity that accommodates polypeptide substrates[1–3]. Chaperonin-mediated protein folding is critically dependent on the closure of a built-in lid[4,5], which is triggered by ATP hydrolysis[6]. The structural rearrangements and molecular events leading to lid closure are still unknown. Here we report four single particle cryo-electron microscopy (cryo-EM) structures of Mm-cpn, an archaeal group II chaperonin[5,7], in the nucleotide-free (open) and nucleotide-induced (closed) states. The 4.3 Å resolution of the closed conformation allowed building of the first ever atomic model directly from the single particle cryo-EM density map, in which we were able to visualize the nucleotide and more than 70% of the side chains. The model of the open conformation was obtained by using the deformable elastic network modelling with the 8 Å resolution open-state cryo-EM density restraints. Together, the open and closed structures show how local conformational changes triggered by ATP hydrolysis lead to an alteration of intersubunit contacts within and across the rings, ultimately causing a rocking motion that closes the ring. Our analyses show that there is an intricate and unforeseen set of interactions controlling allosteric communication and inter-ring signalling, driving the conformational cycle of group II chaperonins. Beyond this, we anticipate that our methodology of combining single particle cryo-EM and computational modelling will become a powerful tool in the determination of atomic details involved in the dynamic processes of macromolecular machines in solution.**

Chaperone-mediated protein folding is critical for the survival and proper function of cells[8]. Impairment of this process has been implicated in a variety of diseases including neurodegeneration, heart disease and cancer[9]. The eukaryotic hetero-oligomeric chaperonin TRiC (also known as CCT) belongs to a unique class of molecular chaperones that assist the folding of an essential subset of cellular proteins with complex topologies, including many cell cycle regulators and cytoskeletal proteins[10]. Recent work suggests that the eukaryotic chaperonin is a potent inhibitor of huntingtin aggregation and toxicity[11,12].

Chaperonins consist of two back-to-back rings with a total of 14–18 subunits. Each subunit is composed of three domains: an equatorial domain that binds ATP and provides inter-ring contacts, an apical domain that binds the substrate, and an intermediate hinge domain[4,13]. All chaperonins use ATP hydrolysis to drive a conformational cycle that encapsulates folding substrates within a central chamber[14,15]. On the basis of the mechanism of encapsulation, chaperonins can be separated into two related, but distinct groups. Group I chaperonins, mostly found in bacteria and endosymbiotic organelles (such as GroEL), have a co-factor (GroES) serving as a detachable lid that binds the apical domains and closes the chamber. Group II chaperonins, found in archaea and eukaryotes, have a built-in lid segment protruding from each apical domain. The molecular mechanism of lid closure in group II chaperonins is virtually unknown, owing in large measure to the lack of high resolution structures for the different states in the conformational cycle.

Here we derive the structures of a group II chaperonin in both open (nucleotide-free) and closed (ATP-induced) states, at unprecedented resolutions by single particle cryo-EM and computational modelling. Our analysis shows that in group II chaperonins the key structural rearrangements leading from the open to closed state are completely different from those found in group I chaperonins, despite structural similarities between the groups.

The 16-subunit homo-oligomeric chaperonin from the mesophilic archaea *Methanococcus maripaludis* (Mm-cpn) provides a simple and tractable model for understanding group II chaperonins[5,7,16]. Mm-cpn folds proteins in an ATP-dependent manner, and shares the allosteric regulation properties of eukaryotic chaperonins such as TRiC[5,7]. A variant of Mm-cpn lacking the built-in lid (here termed 'lidless Mm-cpn') can still bind unfolded polypeptides and hydrolyse ATP, but is unable to mediate folding of a stringent substrate[5]. Because the structural analysis of the nucleotide-free state was dominated by end-on views of the wild-type particles on an electron microscope grid, probably owing to the exposed hydrophobic interior of the open lid, we used lidless Mm-cpn (which has random orientations on the electron microscope grid) for the cryo-EM structural investigation of the poorly understood open state of group II chaperonins.

Two-dimensional averages of cryo-EM images of wild-type and lidless Mm-cpn show that they transition uniformly from an open, nucleotide-free state to a closed conformation after incubation with ATP–$AlF_x$ (Supplementary Fig. 1). These observations contrast with previous findings[17], and suggest that ATP hydrolysis may yield a defined three-dimensional conformation of Mm-cpn, as observed in the eukaryotic chaperonin TRiC[6,15], thus making high resolution structural determination tractable.

Figure 1a shows the 4.3 and 4.8 Å resolution reconstructions of the wild-type and lidless Mm-cpn, respectively, in the ATP-induced closed state (Supplementary Fig. 2e). Both wild-type and lidless Mm-cpn achieved essentially the same closed structure (Fig. 1a).

[1]Graduate Program in Structural and Computational Biology and Molecular Biophysics, [2]National Center for Macromolecular Imaging, Verna and Marrs McLean Department of Biochemistry and Molecular Biology, Baylor College of Medicine, Houston, Texas 77030, USA. [3]Department of Structural Biology, [4]Department of Biology and BioX Program, Stanford University, Stanford, California 94305, USA. †Present addresses: Institut für Strukturbiologie und Biophysik (ISB-3), Forschungszentrum Jülich, 52425 Jülich, Germany (G.F.S.); Max-Planck-Institut für terrestrische Mikrobiologie, Karl-von-Frisch Strasse, 35043 Marburg, Germany (S.R.).

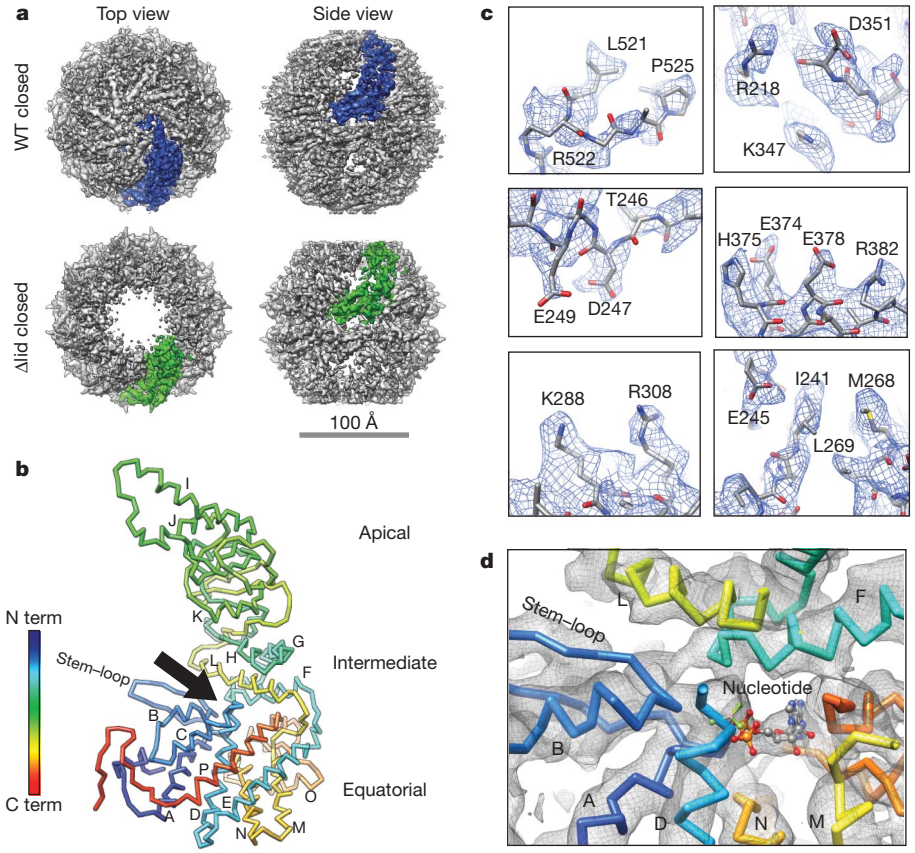


**Figure 1 | Cryo-EM structures of wild-type and lidless Mm-cpn in the closed state.** **a**, Top and side views of the cryo-EM density maps with one subunit coloured blue (wild-type, WT) and green (lidless, Δlid) at 4.3 and 4.8 Å resolution, respectively. **b**, Backbone model of the wild-type closed-state Mm-cpn subunit. The black arrow indicates the nucleotide-binding pocket. Helices are labelled from A to P. **c**, Examples of visible side-chain densities (blue mesh) in the wild-type Mm-cpn map. **d**, Map and backbone model around the nucleotide-binding pocket in **b**.

The resolution of the wild-type closed-state map is sufficient to permit unambiguous segmentation of the density of each subunit (Supplementary Movie 1), as well as the modelling of the Mm-cpn subunits from residues 1 to 532 (Fig. 1b and Supplementary Movie 2). The α-helix pitch and β-strand separation are clearly visible in the density map, as expected at this resolution[18] (Supplementary Fig. 3). Notably, more than 70% of side-chain densities are visible in the map, with more than one-quarter (143 out of 532) fully visible (Fig. 1c, Supplementary Fig. 4 and Supplementary Movie 3). These features allowed for the construction of, to our knowledge, the first atomic model built directly from the cryo-EM density without the aid of a crystal—a feat not yet carried out in previous near-atomic resolution single particle cryo-EM studies[19–22]. Furthermore, density probably representing nucleotide in the ATP-binding pocket is also seen in close contact with α-helices A, B, D, F, L and the end of the 'stem–loop'[4] (Fig. 1d).

In the absence of nucleotide, both chaperonin variants were uniformly open (Fig. 2a and Supplementary Fig. 1). An 8-Å resolution map of Mm-cpn open state was reconstructed from images of nucleotide-free lidless Mm-cpn. The resolution of this open-state map is probably limited by the structural flexibility of the chaperonin (Supplementary Movie 4). The flexibility seems highest in the apical domain, as illustrated in the lidless Mm-cpn map, in which the α-helices are well resolved in the equatorial domain (Fig. 2b) but less resolved in the apical and intermediate domains. This resonates with the structural analysis of group I chaperonins, as the apical domain residues in GroEL crystals have higher B-factors[23], and may reflect the dynamic nature of the substrate-binding sites. In the wild-type Mm-cpn, the open lid tends to cause the chaperonins to orient preferentially with mostly end-on views, accounting for anisotropic sampling of the data, and thus a lower resolution reconstruction of 10 Å (Supplementary Fig. 2e) as shown in another study[24].

As in the closed state, the maps of the lidless and wild-type open-state Mm-cpn are very similar (Fig. 2a), indicating that the presence of the lid does not significantly affect the open conformation. Owing to the clear visibility of secondary structure elements in the 8-Å lidless open-state map, a model for the open-state subunit (Fig. 2c) was built based on the closed-state model and a geometry-constrained, deformable elastic network modelling approach[25] (see Methods).

Given that wild-type and lidless Mm-cpn subunits essentially adopt the same structures for both the open and closed states, we used the models built from the highest resolution maps of the open and closed Mm-cpn states to gain insight into key structural changes accompanying ATP hydrolysis in group II chaperonins. Our analysis shows that the intra- and inter-ring interactions change markedly between the open and closed states.

In the closed state, adjacent subunits within a ring engage in extensive interactions throughout all three domains (Fig. 3a, right). In contrast, neighbouring subunits in the open state are connected primarily through interactions in the equatorial domain (Fig. 3a, left). This may account for the higher flexibility, and lower resolution, of the apical domains in the open state. One of the invariant intra-ring contacts observed in both open and closed states is between Asp 45 and Arg 511 in the adjacent subunits (Supplementary Movie 5). An overlap of these models shows that every subunit within one ring rotates ~40° around this interface during the conformational transition from open to closed state, suggesting that the Asp 45 and Arg 511 residue pair serves as a hinge for intra-ring motion (Fig. 3a, b and Supplementary Movie 5).

Another important component of intra-ring communication is a β-sheet formed between the stem–loop of one subunit and the

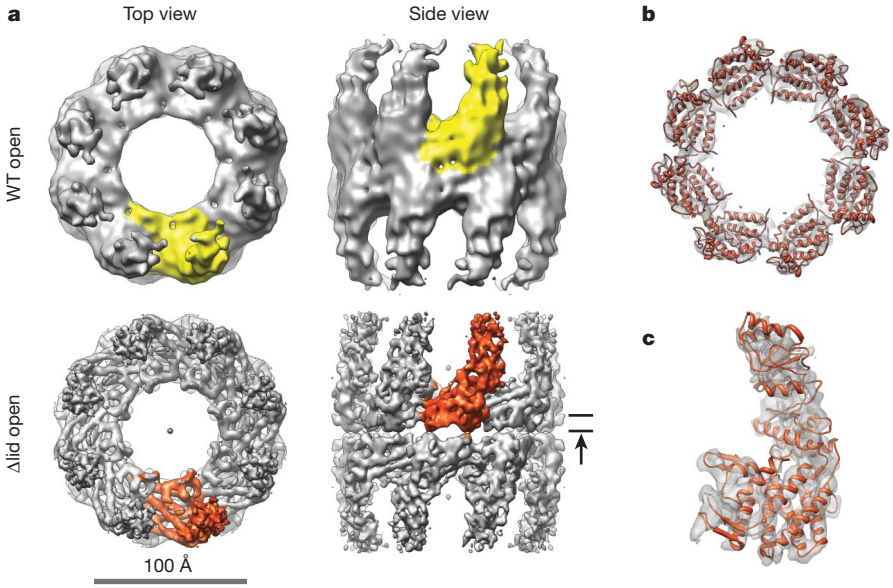


**Figure 2 | Cryo-EM structures of wild-type and lidless Mm-cpn in the open state. a**, Top and side views of the Mm-cpn density maps with one subunit coloured yellow (wild-type) and orange (lidless) at 10 and 8 Å resolution, respectively. **b**, Slice of density map in the equatorial domain of the lidless Mm-cpn open map with α-helices (orange ribbons) fitted into the density. The viewing direction is indicated by the arrow in **a**. **c**, Model of the lidless (orange) open-state Mm-cpn single subunit flexibly fitted into the cryo-EM density map.

amino- and carboxy-terminal segments of the neighbouring subunit (Fig. 3b). Of note, our ability to visualize almost the entire N and C termini (except for the last 11 residues) in the closed state to a level of detail not observed in any previous chaperonin structures[4,13,26,27] uncovered a marked movement of these structural elements during the conformational change of group II chaperonins. In the open state, this β-sheet is tilted upwards, with the visible portions of the flexible N and C termini pointing towards the central chamber of Mm-cpn (Fig. 3a, b, left panels and Supplementary Movie 5). In contrast, these residues are pushed downwards and retracted from the chamber in the closed state (Fig. 3a, b, right panels and Supplementary Movie 5). As a result, the N and C termini become more rigid in the closed state, allowing for visualization and modelling of the complete N terminus and nearly all of the C terminus (up to Gly 532; Fig. 3a, b, right panel).

This structural rearrangement of the termini is supported by differential protease sensitivity observed for the C terminus of lidless Mm-cpn in the open and closed states (Fig. 3c and Supplementary Fig. 6). The N terminus is cleaved at Tyr 15 in both open and closed states, consistent with our models, which predict Tyr 15 to be at the N-terminal β-strand that is further away from the stem–loop (Fig. 3b). In contrast, the C terminus is cleaved at several positions in the open state (Fig. 3c, bands indicated by asterisks), but protected from proteolysis in the closed state, consistent with a highly flexible conformation of the C-terminal tail. The observed protection induced by hydrolysable ATP (Fig. 3a, b) is consistent with our structural conclusion that the C-terminal residues become more rigid in the ATP-induced state. These previously unseen movements of the N and C termini in and out of the chaperonin chamber may contribute to chaperonin mediated folding. Notably, the C terminus

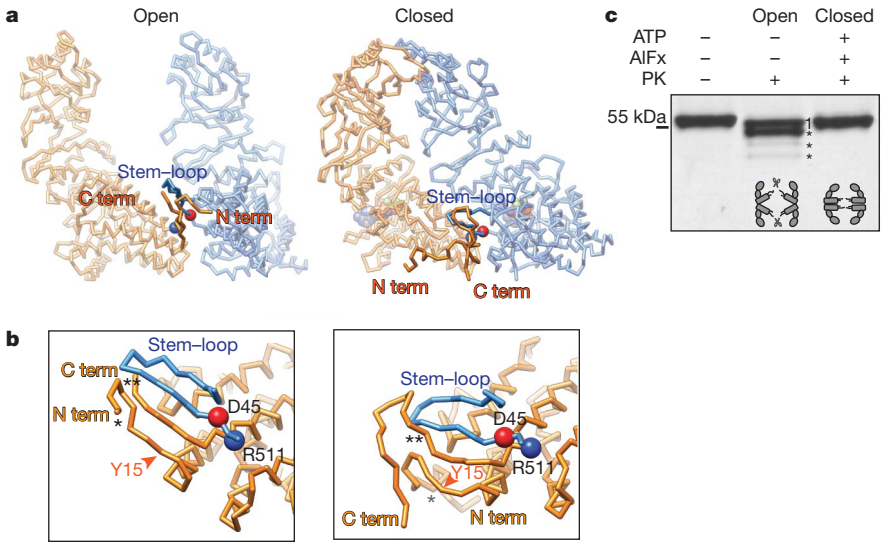


**Figure 3 | Molecular interactions of Mm-cpn subunits within one ring in two states. a**, Backbone models for two neighbouring subunits of two states viewed from the central cavity with nucleotides as sphere models. **b**, Magnified regions of the stem–loop and N and C termini viewed from the right in **a**. Single and double asterisks denote residues Val 7 and Glu 519, respectively, that could be modelled in the open states. **c**, SDS–PAGE gel of protease K treatment of lidless Mm-cpn showing that residues 1–14 get cut for both states (band '1'), and the C terminus can be cut in several locations only for the open state (asterisks).

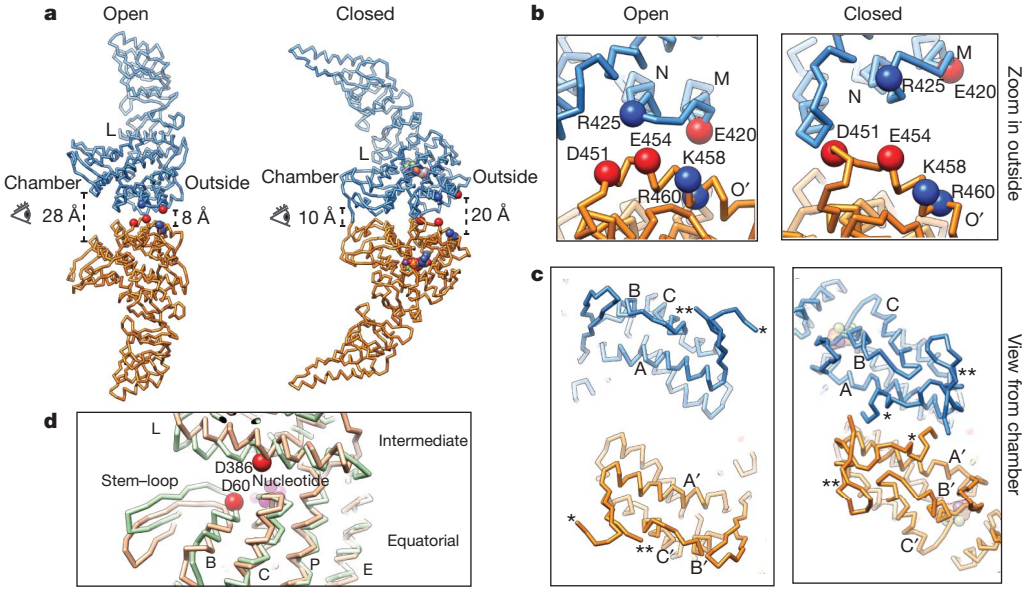


**Figure 4 | Molecular interactions between Mm-cpn subunits across rings in two states and the conformational changes around the nucleotide-binding pocket with some helices labelled.** **a**, Backbone models for two adjacent subunits across the rings of two states. **b**, Insets of the helix O region of two states with positively charged (blue) and negatively charged (red) residues as spheres. **c**, Insets showing the N and C termini viewed by the 'eyes' in **a**. Single and double asterisks have the same definitions as in Fig. 3. **d**, Aligned nucleotide-binding pockets from the closed-state (green) and open-state (orange) models.

of Mm-cpn contains a conserved GGM repeat that is also found in bacterial group I chaperonins[28]. It has been suggested that, in GroEL, these regions have a role in the substrate-folding process[28,29]. Our results provide direct structural evidence for the active involvement of N and C termini in the chaperonin conformational cycle. This 'hand-shaking' structural signature between the N and C termini in one subunit and the stem–loop in the neighbouring subunit may indeed be the key communication between subunits within one ring during ATP hydrolysis (Supplementary Movie 5).

The mode of inter-ring communication in group II chaperonins has remained elusive. Unlike group I chaperonins, where the rings contact in a staggered subunit arrangement[13], all group II chaperonins have a subunit in one ring directly aligned with another subunit in the trans-ring, leading to fully symmetrical and heterologous contacts (Supplementary Fig. 5). Thus, inter-ring communication must occur directly between each pair of contacting subunits across the rings. Our structural analysis shows that the molecular interactions at the ring–ring interface change markedly between the open and closed states (Fig. 4a). In the closed state, the N and C termini of adjacent subunits across the ring are in close proximity (Fig. 4a, c and Supplementary Movie 5), whereas helices M and O′ on the exterior side of the inter-ring interface appear relatively distant. Surprisingly, these contacts change considerably in the open state, with helices M and N in one subunit coming close to helix O′ of the neighbouring subunit across the ring. Our structures suggest that the open state is stabilized by a network of complementary charges linking Arg 425 and Glu 420 in helices M and N with Asp 451, Glu 454, Lys 458 and Arg 460 in helix O′ (Fig. 4b). The open state also causes an extensive motion that separates the N and C termini from the subunits across the rings, thereby pushing the termini towards the respective central chambers (Fig. 4a, c and Supplementary Movie 5). Such a conformational switch of the termini also makes them more susceptible to protease digestion in the open state (Fig. 3c).

This analysis indicates that transition between the open and closed states in group II chaperonins involves a rocking motion that markedly rearranges the inter-ring contacts. This movement differs radically from that observed in group I chaperonins[26]. This difference in inter-ring communication could result from the in-register ring–ring arrangement of group II chaperonins (Supplementary Fig. 5), which allows greater freedom of tilting for the equatorial domains compared to the arrangement in GroEL. The staggered arrangement of inter-ring subunits in group I chaperonins leads to the relative conservation of inter-ring contacts throughout the conformational cycle. This quaternary structural feature in group II chaperonins may compensate for the lack of a lid-like GroES co-chaperonin and allow self-closure of the folding chamber through subunit rocking mediated by equatorial domain rotation.

A major question in understanding nanomachines driven by ATP hydrolysis is how local changes in the nucleotide-binding site are communicated globally throughout the protein. The previous structures of group II chaperonins[15,17,24] did not show how ATP hydrolysis affects intra- and inter-ring communication. Our ability to identify how secondary structure elements move in response to ATP hydrolysis allows us to propose how local changes in the nucleotide-binding site can be propagated within and between rings. Our maps clearly indicate that helix L in the intermediate domain tilts in response to ATP hydrolysis (Fig. 4d). As a result, the distal C-terminal end of helix L moves towards the stem–loop. Concurrently, a concerted movement of contiguous helices L, M and N causes M and N to be farther away from the O′ helix of the subunit across the ring (Fig. 4a, b). Together, these molecular events produce the forward rocking of the equatorial domain towards the centre of the cavity, which is transmitted through the intermediate domain to the apical domain, thus closing the lid[15]. The effect of ATP hydrolysis on helix L and this stem–loop fits with the observation that Asp 386 in helix L and Asp 60 at the end of the stem–loop both contact the γ-phosphate mimic $AlF_x$ in the closed thermosome crystal structure[4] (Fig. 4d).

Our single particle cryo-EM analysis of Mm-cpn has shown unprecedented detail of the open and closed states of group II chaperonins. The structural rearrangements observed here are markedly different from those occurring in the well-studied group I chaperonins[26], indicating that a completely different mechanism of inter-subunit communication drives the folding cycles in group II chaperonins.

## METHODS SUMMARY

Wild-type and lidless Mm-cpn were expressed and purified from *Escherichia coli*[5]. Specimens were prepared for the cryo-EM experiments by rapid freezing using the Vitrobot (FEI). All imaging was done on a JEM3200FSC electron microscope (JEOL) with an in-column energy filter except for the wild-type

open state, which was imaged on a JEM2010F electron microscope. All data was recorded with Gatan 4k × 4k CCD cameras (model no. 895). The particle images were processed using the standard EMAN procedures[30] with D8 symmetry imposed. The resolution of the reconstruction was assessed using the 0.5 Fourier shell correlation criterion. The number of particles used for three-dimensional reconstruction for wild-type closed, lidless closed, wild-type open and lidless open states were 29,926, 24,434, 27,598 and 18,168 respectively. The starting models for the Mm-cpn open and closed states were built from its homologue thermosome KS-1 (Protein Data Bank (PDB) accession 1Q3Q). The model for the closed state was hand-built by crystallographic model building tool (see Methods). The model for the open state was refined with a deformable elastic network algorithm using DireX[25].

**Full Methods** and any associated references are available in the online version of the paper at www.nature.com/nature.

**Received 24 June; accepted 16 November 2009.**

1. Bukau, B. & Horwich, A. L. The Hsp70 and Hsp60 chaperone machines. *Cell* **92,** 351–366 (1998).
2. Frydman, J. Folding of newly translated proteins *in vivo*: the role of molecular chaperones. *Annu. Rev. Biochem.* **70,** 603–647 (2001).
3. Hartl, F. U. & Hayer-Hartl, M. Molecular chaperones in the cytosol: from nascent chain to folded protein. *Science* **295,** 1852–1858 (2002).
4. Ditzel, L. *et al.* Crystal structure of the thermosome, the archaeal chaperonin and homolog of CCT. *Cell* **93,** 125–138 (1998).
5. Reissmann, S., Parnot, C., Booth, C. R., Chiu, W. & Frydman, J. Essential function of the built-in lid in the allosteric regulation of eukaryotic and archaeal chaperonins. *Nature Struct. Mol. Biol.* **14,** 432–440 (2007).
6. Meyer, A. S. *et al.* Closing the folding chamber of the eukaryotic chaperonin requires the transition state of ATP hydrolysis. *Cell* **113,** 369–381 (2003).
7. Kusmierczyk, A. R. & Martin, J. Nucleotide-dependent protein folding in the type II chaperonin from the mesophilic archaeon Methanococcus maripaludis. *Biochem. J.* **371,** 669–673 (2003).
8. Dobson, C. M. Principles of protein folding, misfolding and aggregation. *Semin. Cell Dev. Biol.* **15,** 3–16 (2004).
9. Balch, W. E., Morimoto, R. I., Dillin, A. & Kelly, J. W. Adapting proteostasis for disease intervention. *Science* **319,** 916–919 (2008).
10. Yam, A. Y. *et al.* Defining the TRiC/CCT interactome links chaperonin function to stabilization of newly made proteins with complex topologies. *Nature Struct. Mol. Biol.* **15,** 1255–1262 (2008).
11. Tam, S., Geller, R., Spiess, C. & Frydman, J. The chaperonin TRiC controls polyglutamine aggregation and toxicity through subunit-specific interactions. *Nature Cell Biol.* **8,** 1155–1162 (2006).
12. Kitamura, A. *et al.* Cytosolic chaperonin prevents polyglutamine toxicity with altering the aggregation state. *Nature Cell Biol.* **8,** 1163–1169 (2006).
13. Braig, K. *et al.* The crystal structure of the bacterial chaperonin GroEL at 2.8 Å. *Nature* **371,** 578–586 (1994).
14. Saibil, H. R. *et al.* ATP induces large quaternary rearrangements in a cage-like chaperonin structure. *Curr. Biol.* **3,** 265–273 (1993).
15. Booth, C. R. *et al.* Mechanism of lid closure in the eukaryotic chaperonin TRiC/CCT. *Nature Struct. Mol. Biol.* **15,** 746–753 (2008).
16. Kusmierczyk, A. R. & Martin, J. Nested cooperativity and salt dependence of the ATPase activity of the archaeal chaperonin Mm-cpn. *FEBS Lett.* **547,** 201–204 (2003).
17. Clare, D. K. *et al.* Multiple states of a nucleotide-bound group 2 chaperonin. *Structure* **16,** 528–534 (2008).
18. Blow, D. *Outline of Crystallography for Biologists* (Oxford Univ. Press, 2002).
19. Ludtke, S. J. *et al.* De novo backbone trace of GroEL from single particle electron cryomicroscopy. *Structure* **16,** 441–448 (2008).
20. Jiang, W. *et al.* Backbone structure of the infectious ε15 virus capsid revealed by electron cryomicroscopy. *Nature* **451,** 1130–1134 (2008).
21. Zhang, X. *et al.* Near-atomic resolution using electron cryomicroscopy and single-particle reconstruction. *Proc. Natl Acad. Sci. USA* **105,** 1867–1872 (2008).
22. Yu, X., Jin, L. & Zhou, Z. H. 3.88 Å structure of cytoplasmic polyhedrosis virus by cryo-electron microscopy. *Nature* **453,** 415–419 (2008).
23. Braig, K., Adams, P. D. & Brünger, A. T. Conformational variability in the refined structure of the chaperonin GroEL at 2.8 Å resolution. *Nature Struct. Biol.* **2,** 1083–1094 (1995).
24. Schoehn, G., Hayes, M., Cliff, M., Clarke, A. R. & Saibil, H. R. Domain rotations between open, closed and bullet-shaped forms of the thermosome, an archaeal chaperonin. *J. Mol. Biol.* **301,** 323–332 (2000).
25. Schröder, G. F., Brunger, A. T. & Levitt, M. Combining efficient conformational sampling with a deformable elastic network model facilitates structure refinement at low resolution. *Structure* **15,** 1630–1641 (2007).
26. Xu, Z., Horwich, A. L. & Sigler, P. B. The crystal structure of the asymmetric GroEL–GroES–$(ADP)_7$ chaperonin complex. *Nature* **388,** 741–750 (1997).
27. Boisvert, D. C., Wang, J., Otwinowski, Z., Horwich, A. L. & Sigler, P. B. The 2.4 Å crystal structure of the bacterial chaperonin GroEL complexed with ATPγS. *Nature Struct. Biol.* **3,** 170–177 (1996).
28. Tang, Y. C. *et al.* Structural features of the GroEL-GroES nano-cage required for rapid folding of encapsulated protein. *Cell* **125,** 903–914 (2006).
29. Suzuki, M. *et al.* Effect of the C-terminal truncation on the functional cycle of chaperonin GroEL: implication that the C-terminal region facilitates the transition from the folding-arrested to the folding-competent state. *J. Biol. Chem.* **283,** 23931–23939 (2008).
30. Ludtke, S. J., Baldwin, P. R. & Chiu, W. EMAN: semiautomated software for high-resolution single-particle reconstructions. *J. Struct. Biol.* **128,** 82–97 (1999).

**Supplementary Information** is linked to the online version of the paper at www.nature.com/nature.

**Acknowledgements** We acknowledge the support of grants from the National Institutes of Health through the Nanomedicine Development Center Roadmap Initiative, Biomedical Technology Research Center for Structural Biology in National Center for Research Resources, Nanobiology Training Fellowship administered by the Keck Center of the Gulf Coast Consortia and the National Science Foundation.

**Author Contributions** J.Z. and J.J. collected the cryo-EM image data. J.Z. performed the image processing and reconstructions with the assistance of C.J.F. M.L.B. did the modelling and analysis of the closed state. G.F.S. did the model fitting for the open state. N.R.D. and S.R. designed the lidless mutation, the biochemical conditions for the cryo-EM experiments and performed all biochemical characterizations and experiments. S.J.L. advised on data processing and map filtering. J.Z., N.R.D., M.L.B., G.F.S., J.F. and W.C. interpreted the structural results. M.D., W.C. and J.Z. prepared all the movies. All authors contributed to the preparation of the manuscript.

**Author Information** The three-dimensional cryo-EM density maps have been deposited into the EBI-MSD EMD database with accession codes: EMD-5137 (wild-type closed), EMD-5138 (lidless closed), EMD-5139 (wild-type open) and EMD-5140 (lidless open). The atomic models have been deposited in the Protein Data Bank as 3IYE (wild-type closed) and 3IYF (lidless open). Reprints and permissions information is available at www.nature.com/reprints. The authors declare no competing financial interests. Correspondence and requests for materials should be addressed to W.C. (wah@bcm.edu) or J.F. (jfrydman@stanford.edu).

## METHODS

**Mm-cpn purification and cryo-specimen preparation.** Both wild-type and lidless Mm-cpn were purified in buffer (20 mM HEPES, pH 7.4, 50 mM NaCl, 5 mM MgCl, 0.1 mM EDTA, 1 mM dithiothreitol (DTT), 10% glycerol and 0.1 mM phenylmethylsulphonyl fluoride (PMSF)). They were then diluted in ATPase buffer (20 mM Tris-HCl, pH 7.5, 100 mM KCl, 5 mM MgCl and 1 mM DTT) to lower the glycerol concentration. Detergent octyl glucoside (0.05%) was added to the open state of wild-type Mm-cpn buffer before cryo-EM freezing to yield more side views.

For the nucleotide-induced states of wild-type and lidless Mm-cpn, a 1 mM final concentration of ATP–$AlF_x$ was used. The sample was then incubated in a water bath at 37 °C for 1 h before freezing onto the grid. This nucleotide concentration is high enough to overcome the negative cooperativity of ATP hydrolysis between two rings[5], thus, obtaining a more homogeneous closed-state Mm-cpn for high resolution structure determination. The nucleotide-free Mm-cpn was incubated at 37 °C for 10 min before freezing onto the grid.

Samples were embedded in vitreous ice as follows. A 2.5-μl aliquot of the above-prepared samples was applied onto a 400-mesh R1.2/1.3 Quantifoil grid (Quantifoil Micro Tools). The grid was previously washed and glow discharged. After applying the sample, the grid was blotted and rapidly frozen in liquid ethane using a Vitrobot (FEI), and stored in liquid nitrogen before imaging.

**Proteinase K protection assay.** Mm-Cpn was incubated with proteinase K as previously described, with slight modifications[5]. To generate $AlF_x$, 1 mM $Al(NO_3)_3$ and 6 mM NaF were added to the reaction, then incubated at 37 °C for 10 min. The chaperonin was incubated with 20 μg $ml^{-1}$ proteinase K for 5 min at 25 °C, then 5 mM PMSF was added to inhibit the proteinase K activity. After completion of the digestion, the reactions were placed on ice for 5 min, then analysed by SDS–PAGE.

**Cryo-EM data collection.** The lidless Mm-cpn open and closed states and the wild-type Mm-cpn closed state were imaged on a JEM3200FSC electron cryomicroscope operated at 300 kV, whereas the wild-type open state was imaged on a JEM2010F electron microscope at 200 kV (JEOL). Both microscopes are equipped with a field emission gun. Images from JEM3200FSC and JEM2010F were recorded at a detector magnification of ×112,000 and ×83,100, respectively, on Gatan 4k × 4k CCD cameras (model no. 895, Gatan). For the JEM3200FSC data collection, an in-column omega energy filter was used with a slit width of 10 eV. The particle images for the 4.3 Å resolution map of the wild-type closed state were obtained from 616 CCD frames using two grids with a defocus range of 1–2.5 μm.

**Cryo-EM data processing.** All the particle images were selected automatically using the EMAN[30] program batchboxer and then manually screened using the EMAN program boxer. The class averages show that they are conformationally uniform (Supplementary Fig. 1), in contrast to an earlier report showing multiple conformations in the apo state[17]. The contrast transfer function (CTF) parameters of these particles were first fitted using the automatic CTF fitting program fitctf.py[31], and then manually examined and adjusted using the EMAN program ctfit.

All particles were phase-flipped, and then an initial model for each of the four states was generated using the EMAN program startcsym. These four models were further refined against the corresponding particle images using the standard EMAN iterative reconstruction algorithm[30,32] with D8 symmetry imposed. The final resolutions of wild-type closed, lidless closed, wild-type open and lidless open state density maps were 4.3 Å, 4.8 Å, 10 Å and 8 Å, respectively, according to the Fourier shell correlation[33] with 0.5 cut-off criterion (Supplementary Fig. 2e).

**Cryo-EM map post-processing and visualization.** To optimize feature contrast in the final maps used for atomistic model building, a one-dimensional structure factor was computed from the Cα model derived from the unfiltered final reconstruction, and imposed on the map. This 'optimally filtered' map was then low-pass filtered to the point at which visible noise was not apparent (see later for details). Similar map-filtering techniques have been suggested earlier[34,35]. Map segmentation, visualizations and animations are done in Chimera[36] and Amira (Visage Imaging).

**Closed-state model building.** Initially, a homology model for Mm-cpn was constructed using thermosome KS-1 (PDB accession 1Q3Q) as a template with Swiss-Model[37]. The Cα backbone of this model was then adjusted to fit the cryo-EM map density using Coot[38] and Gorgon (http://www.cs.wustl.edu/~ssa1/gorgon). Secondary structure elements and protruding side-chain densities were used to anchor the Cα atoms in the model. Using EMAN, this model was then blurred to 4.5 Å resolution, from which a one-dimensional structure factor curve was calculated and used to scale the structure factor amplitudes of the density map. In this amplitude-scaled map, side-chain densities became more resolved and allowed for atomic modelling. As side-chain density was visible, it was then possible to optimize the fit of the model, including main-chain and side-chain atoms. Registration of secondary structure elements within the density was first performed, followed by optimization of loop and side-chain placement throughout the density. During this process, a strategy similar to the X-ray crystallographic approach was used to improve the Mm-cpn model quality by optimizing bond lengths, bond angles, dihedral angles and rotamer assignment. Initial model quality estimations were obtained by examining the Ramachandran plot using MolProbity[39]. To assess the map and model, we classified each amino acid into one of the four possible categories. 'Fully resolved' side chains were termed as those in which the local shape of the density matched well to the model side-chain rotamers. 'Partially resolved' side chains had side chains that fall within but do not necessarily fit completely to an envelope of protruding density. 'Ambiguous' side chains had ambiguous fits of the Cα and side-chain atoms to the density. Glycines belong to the final category that has no side chain (Supplementary Fig. 4)

**Open-state model building.** The open-state lidless Mm-cpn model was obtained by real-space refinement with the program DireX[25] using the homology model of the closed state as a starting model. DireX uses a geometry-based conformational sampling algorithm and the deformable elastic network (DEN) restraints plus the forces from the density map to maximize the correlation between the experimental density map and a density map computed from the model (see Supplementary Methods).

The actual refinement for the open state Mm-cpn model was performed in two steps: first, strong non-deformable DEN restraints were used to obtain a fit with almost rigid subunits. In the second step, the DEN restraints were made weaker and deformable for flexibly refining the models. To account for missing experimental density in regions of high flexibility, residue-based B-factors were taken from the thermosome crystal structure (PDB accession 1Q3Q), assigned to the homology model and used to scale the contribution of each residue to the model map. This reduced artificial structural distortions due to missing or significantly decreased density.


31. Yang, C. *et al.* Estimating contrast transfer function and associated parameters by constrained nonlinear optimization. *J. Microsc.* **233,** 391–403 (2009).
32. Ludtke, S. J., Jakana, J., Song, J.-L., Chuang, D. & Chiu, W. A 11.5 Å single particle reconstruction of GroEL using EMAN. *J. Mol. Biol.* **314,** 253–262 (2001).
33. Harauz, G. & van Heel, M. Exact filters for general geometry three dimensional reconstruction. *Optik* **73,** 146–156 (1986).
34. Fernández, J. J., Luque, D., Caston, J. R. & Carrascosa, J. L. Sharpening high resolution information in single particle electron cryomicroscopy. *J. Struct. Biol.* **164,** 170–175 (2008).
35. Rosenthal, P. B. & Henderson, R. Optimal determination of particle orientation, absolute hand, and contrast loss in single-particle electron cryomicroscopy. *J. Mol. Biol.* **333,** 721–745 (2003).
36. Pettersen, E. F. *et al.* UCSF Chimera—a visualization system for exploratory research and analysis. *J. Comput. Chem.* **25,** 1605–1612 (2004).
37. Arnold, K., Bordoli, L., Kopp, J. & Schwede, T. The SWISS-MODEL workspace: a web-based environment for protein structure homology modelling. *Bioinformatics* **22,** 195–201 (2006).
38. Emsley, P. & Cowtan, K. Coot: model-building tools for molecular graphics. *Acta Crystallogr. D* **60,** 2126–2132 (2004).
39. Lovell, S. C. *et al.* Structure validation by Cα geometry: ϕ, ψ and Cβ deviation. *Proteins* **50,** 437–450 (2003).